

Beyond Conventional Ferromagnetism and Antiferromagnetism: A Phase with Nonrelativistic Spin and Crystal Rotation Symmetry

Libor Šmejkal,^{1,2} Jairo Sinova,^{1,2} and Tomas Jungwirth^{2,3}

¹*Institut für Physik, Johannes Gutenberg Universität Mainz, 55128, Mainz, Germany*

²*Institute of Physics, Czech Academy of Sciences, Cukrovarnická 10, 162 00, Praha 6, Czech Republic*

³*School of Physics and Astronomy, University of Nottingham, NG7 2RD, Nottingham, United Kingdom*



(Received 6 February 2022; revised 6 April 2022; accepted 11 August 2022; published 23 September 2022)

Recent series of theoretical and experimental reports have driven attention to time-reversal symmetry-breaking spintronic and spin-splitting phenomena in materials with collinear-compensated magnetic order incompatible with conventional ferromagnetism or antiferromagnetism. Here we employ an approach based on nonrelativistic spin-symmetry groups that resolves the conflicting notions of unconventional ferromagnetism or antiferromagnetism by delimiting a third basic collinear magnetic phase. We derive that all materials hosting this collinear-compensated magnetic phase are characterized by crystal-rotation symmetries connecting opposite-spin sublattices separated in the real space and opposite-spin electronic states separated in the momentum space. We describe prominent extraordinary characteristics of the phase, including the alternating spin-splitting sign and broken time-reversal symmetry in the nonrelativistic band structure, the planar or bulk d -, g -, or i -wave symmetry of the spin-dependent Fermi surfaces, spin-degenerate nodal lines and surfaces, band anisotropy of individual spin channels, and spin-split general, as well as time-reversal invariant momenta. Guided by the spin-symmetry principles, we discover in *ab initio* calculations outlier materials with an extraordinary nonrelativistic spin splitting, whose eV-scale and momentum dependence are determined by the crystal potential of the nonmagnetic phase. This spin-splitting mechanism is distinct from conventional relativistic spin-orbit coupling and ferromagnetic exchange, as well as from the previously considered anisotropic exchange mechanism in compensated magnets. Our results, combined with our identification of material candidates for the phase ranging from insulators and metals to a parent crystal of cuprate superconductors, underpin research of novel quantum phenomena and spintronic functionalities in high-temperature magnets with light elements, vanishing net magnetization, and strong spin coherence. In the discussion, we argue that the conflicting notions of unconventional ferromagnetism or antiferromagnetism, on the one hand, and our symmetry-based delimitation of the third phase, on the other hand, favor a distinct term referring to the phase. The alternating spin polarizations in both the real-space crystal structure and the momentum-space band structure characteristic of this unconventional magnetic phase suggest a term *altermagnetism*. We point out that d -wave *altermagnetism* represents a realization of the long-sought-after counterpart in magnetism of the unconventional d -wave superconductivity.

DOI: [10.1103/PhysRevX.12.031042](https://doi.org/10.1103/PhysRevX.12.031042)

Subject Areas: Condensed Matter Physics,
Magnetism, Spintronics

I. INTRODUCTION

Recent predictions of time-reversal symmetry breaking [1–3] and spin splitting [1,2,4–12] in electronic bands, typical of ferromagnets, in materials with collinear-compensated magnetic order, typical of antiferromagnets, are incompatible with the conventional division into the

ferromagnetic and antiferromagnetic phases. The consequences of the intriguing electronic structure of these collinear-compensated magnets have been illustrated by predictions of odd-under-time-reversal responses, including anomalous Hall and Kerr effects [1–3,9,13–15], as well as spin current, giant and tunneling magnetoresistance, and spin-torque phenomena [6,11,12,16–18]. Some of the predictions of these unexpected responses have been already supported by experiments [9,19–22].

In this article, we resolve the conflicting notions of unconventional ferromagnetism or unconventional antiferromagnetism by deriving that on the basic level of uncorrelated nonrelativistic nonfrustrated (collinear) magnetism,

Published by the American Physical Society under the terms of the [Creative Commons Attribution 4.0 International license](https://creativecommons.org/licenses/by/4.0/). Further distribution of this work must maintain attribution to the author(s) and the published article's title, journal citation, and DOI.

symmetry allows for three instead of two distinct phases. We employ a symmetry approach based on a nonrelativistic spin-group formalism [23–25]. To explain its merits, we first recall the conventional theory frameworks.

A traditional approach to the basic categorization of a magnetic materials phases based on models focusing on spatial and spin arrangements of magnetic atoms alone while omitting nonmagnetic atoms in the lattice can be traced back to the seminal works on Néel’s collinear antiferromagnetism [26]. Subsequently, the approach was employed, e.g., when discussing the competition of Néel’s antiferromagnetism and the spin-liquid phase in the context of high-temperature cuprate superconductors [27]. Recently, models considering clusters of magnetic atoms have underpinned the multipole theory of the anomalous Hall effect in noncollinear-compensated magnets [28], and of the nonrelativistic spin splitting in collinear-compensated magnets [5,8]. However, these models are principally incapable of providing a general classification and description of the underlying magnetic phases in prominent families of materials. A specific example is rutile crystals with the collinear-compensated magnetic order [1,4,7], in which the nonmagnetic atoms have been recognized to play a key role in the anomalous time-reversal symmetry-breaking spin phenomena [1,3]. In particular, RuO_2 is a prominent room-temperature metallic member of this rutile family, in which the unconventional spin physics and spintronics have already been studied both theoretically and experimentally [1,4,16–18,20–22].

A traditional symmetry description of the full structure of magnetic crystals, including the nonmagnetic atoms, considers transformations in coupled real physical space and the space of magnetic moment vectors. In other words, the transformations acting on the coordinates of the atoms, subject to the standard crystallographic restrictions, simultaneously act on the components of the magnetic moment vectors [24,25,29] (see Supplemental Material Sec. I Fig. S1 [30]). This symmetry formalism naturally arises from the classical orbital-current model of magnetic moments [31], as well as from the relativistic quantum-mechanical description of coupled spin and orbital degrees of freedom of electrons [31,32]. The corresponding magnetic groups [29,31,33–35] have been broadly applied in the research of equilibrium and nonequilibrium phenomena, including their modern topological variants [36–38], and have represented the primary tool for a systematic classification of hundreds of magnetic structures in materials databases [35,39].

Magnetic groups are indispensable for the description of effects governed by relativistic physics. However, the inherent relativistic nature of the magnetic-group symmetry transformations in coupled real and spin space makes the magnetic groups generally unsuitable for the classification of nonrelativistic phenomenology, which typically plays the leading role in magnetism [23,40]. Magnetic space

groups of type II describing time-reversal invariant crystals without a magnetic order, are an exception for which a transition to a nonrelativistic physics description in decoupled spin and real space can be generally performed by making a direct product with the $\text{SU}(2)$ group of spin-space rotation transformations [24,28]. For the remaining magnetic space groups of types I, III, and IV encompassing collinear as well as noncollinear magnets [7,10], a transition to the nonrelativistic physics description is not available [5,8,28]. Therefore, the strong nonrelativistic spin-splitting phenomena are not generally described by magnetic groups augmented by spin-space transformations [7,10].

In this article, we use an approach to rigorously and systematically classify and describe nonrelativistic magnetic materials phases and their physical properties based on the spin-group formalism [23–25] of symmetry transformations in decoupled real and spin space. The spin groups are a generalization of the conventional magnetic groups [23–25]. They consider pairs of transformations $[R_i || R_j]$, where the transformations on the left of the double vertical bar act only on the spin space and on the right of the double vertical bar only on the real space [23–25] (see Supplemental Material Sec. I Fig. S1 [30]). The symmetry landscape of the spin groups is much richer because, in general, different rotation transformations can simultaneously act on the spin and real space, and only the transformations in the real space are crystallographically restricted. (The same rotation transformations simultaneously acting on the spin and real space are contained in both magnetic and spin groups.) Despite their richness, studies based on the spin symmetries have appeared only sporadically in the literature. For example, in the past they were used for the classification of possible spin arrangements on crystals and spin dynamics, with an emphasis on complex noncollinear or disordered structures, while not focusing on the electronic structure [40]. Very recently, they have been applied in studies of magnons [41] or topological quasiparticles [42–45]. Overall, however, the spin-group formalism has remained largely unexploited and undeveloped [46].

The nonrelativistic spin groups represent an example of approximate or so-called “hidden” symmetries in the sense that relativistic effects are generally present in all magnets. The key significance of the nonrelativistic spin groups is that they can offer a systematic symmetry description of physics that is commonly leading in magnetism and that arises from the strong nonrelativistic electromagnetic crystal potentials [23,40]. Here, by the electric crystal potential, we refer to the internal potential in the nonmagnetic phase of the crystal, as described, e.g., by the local density approximation of the density-functional theory (DFT); by the additional magnetic component, we refer to the modification of the internal crystal potential due to the transition to the magnetically ordered phase. Since the magnetic groups represent only a small subset of the spin groups [25], they are prone to omitting prominent magnetic phases

dominated by the nonrelativistic electromagnetic crystal potentials. For example, the magnetic groups, which generally encompass collinear and noncollinear magnets, can determine only whether a net magnetization is allowed or not, but do not distinguish ferromagnets from antiferromagnets in which magnetization arises only as a weak relativistic perturbation [31]. For the band structures, the magnetic groups can be used to identify a violation of Kramers spin degeneracy [10,36,47–52]. However, both the magnetic-group formalism and Kramers theorem [53,54] entangle nonrelativistic and relativistic physics. Consequently, the nonrelativistic spin splitting in materials from the magnetic groups violating the Kramers spin degeneracy were identified by performing numerical DFT calculations with the relativistic spin-orbit coupling turned off [10].

In our work, by employing and developing the spin-group formalism, we derive three distinct phases of nonrelativistic collinear magnetism: The first phase has one spin lattice (or opposite-spin sublattices not connected by any symmetry transformation). It corresponds to conventional ferromagnetism (ferrimagnetism) [31]. The second phase has opposite-spin sublattices connected by translation or inversion (or both), and corresponds to conventional antiferromagnetism [23,26,41]. The third phase has opposite-spin sublattices connected by rotation (proper or improper and symmorphic or nonsymmorphic) but not connected by translation or inversion. Unlike the conventional ferromagnetic phase with a nonrelativistic magnetization and spin-split bands that break time-reversal symmetry [31], and unlike the conventional antiferromagnetic phase with nonrelativistic spin-degenerate time-reversal invariant bands and zero net magnetization [26,32,55–58], the third phase has split but equally populated spin-up and spin-down energy isosurfaces in the band structure that break time-reversal symmetry. The spin-group formalism allows us to provide a complete classification and description of the specifics of the spin-momentum locking in the band structure of the third phase. Our direct link of the spin groups to real material candidates establishes that the third phase is abundant. We also show that it is a strong, robust, and fundamental phase, as it does not require (but can coexist with) relativistic spin-orbit coupling, electronic correlations, or magnetic fluctuations or frustrations. We point out that our classification and description based on the spin-group formalism are universally applicable to any effective single-particle Kohn-Sham Hamiltonian, as well as for the Dyson-equation description of correlated or disordered systems.

Principles based on the spin-group symmetries guide us to our discovery of outlier materials hosting the third phase, with an extraordinary microscopic spin-splitting mechanism, whose eV scale and momentum dependence are determined by the electric crystal potential, i.e., by the scale and momentum dependence of the band splitting of the

nonmagnetic phase. It is fundamentally distinct from the earlier-considered various internal magnetic-interaction mechanisms [4,7,8,17,59,60], such as the anisotropic spin-dependent hopping in the magnetic state [8,17]. The spin-splitting mechanism in the third magnetic phase by the electric crystal potential is nonrelativistic and accompanied by zero net magnetization. Therefore, it also starkly contrasts with the conventional mechanisms of the ferromagnetic splitting due to the nonzero net magnetization, or the relativistic spin-orbit splitting due to the broken inversion symmetry. It opens a new paradigm for designing spin quantum phases of matter based on the strong crystal-potential effects complementing the widely explored relativistic or many-body correlation phenomena [61].

The focus of our work is on the classification and description of the nonrelativistic band structures of materials hosting the third phase and the identification of new material candidates, which opens a range of potential science and technology implications of this magnetic phase. In the Supplemental Material Sec. I [30], we briefly comment on the links to relativistic effects and noncollinear magnetism [3].

II. DERIVATION OF SPIN-GROUP CATEGORIZATION OF NONRELATIVISTIC COLLINEAR MAGNETISM

We start with the derivation of the three distinct spin-group types describing, respectively, the three nonrelativistic phases of collinear magnets. In general, spin groups can be expressed as a direct product $\mathbf{r}_s \times \mathbf{R}_s$ of so-called spin-only group \mathbf{r}_s containing transformations of the spin space alone, and so-called nontrivial spin groups \mathbf{R}_s containing the elements $[R_i || R_j]$, but no elements of the spin-only group [24,25]. For the collinear spin arrangements on crystals, the spin-only group is given by [24,25] $\mathbf{r}_s = \mathbf{C}_\infty + \bar{\mathbf{C}}_2 \mathbf{C}_\infty$. Here, \mathbf{C}_∞ is a group representing all rotations of the spin space around the common axis of spins, and $\bar{\mathbf{C}}_2$ is a 180° rotation around an axis perpendicular to the spins, combined with the spin-space inversion. We recall that the spin-space inversion in the spin groups enters via the time reversal [24,25,40]. We also again emphasize here that the relativistic magnetic space groups encompass collinear, as well as general noncollinear magnets [7,10]. This implies that, e.g., a conjecture based on the spin-space $\bar{\mathbf{C}}_2$ symmetry that nonrelativistic spin splitting is generally excluded in materials belonging to the type IV magnetic space groups [7,10] is invalid.

The form of the nonrelativistic spin-only group \mathbf{r}_s for collinear magnets has two basic general implications independent of the specific nontrivial spin group \mathbf{R}_s . The first implication follows from \mathbf{C}_∞ . This symmetry makes spin a good quantum number with a common quantization axis independent of the crystal momentum across the nonrelativistic band structure. The electronic

structure is thus strictly separated into nonmixing spin-up and spin-down channels.

The second implication follows from the \bar{C}_2 symmetry in the spin-only group of collinear magnets. Since the spin-space inversion enters via the time reversal [24,25,40], it is accompanied by a time reversal in the real space (\mathcal{T}). Although \mathcal{T} acts as an identity on the real-space coordinates of the atoms, it flips the sign of the crystal momentum. This is important for the band-structure spin symmetries. In particular, we now use the symmetry $[\bar{C}_2|\mathcal{T}]$, which follows directly from the above spin-only group symmetry of the collinear magnets and from the simultaneous action of the time reversal on the spin and real (momentum) space. When applying the transformation $[\bar{C}_2|\mathcal{T}]$ on spin (s) and crystal-momentum (\mathbf{k})-dependent bands $\epsilon(s, \mathbf{k})$, we obtain $[\bar{C}_2|\mathcal{T}]\epsilon(s, \mathbf{k}) = \epsilon(s, -\mathbf{k})$. We see that the $[\bar{C}_2|\mathcal{T}]$ transformation acts the same way on $\epsilon(s, \mathbf{k})$ as the real-space inversion. Next, since $[\bar{C}_2|\mathcal{T}]$ is a symmetry of nonrelativistic collinear spin arrangements on crystals, $[\bar{C}_2|\mathcal{T}]\epsilon(s, \mathbf{k}) = \epsilon(s, \mathbf{k})$, and hence, $\epsilon(s, \mathbf{k}) = \epsilon(s, -\mathbf{k})$. We derive that the nonrelativistic bands of all collinear magnets are invariant under real-space (crystal-momentum) inversion not only in inversion-symmetric collinear magnets [1,7,8], but even if the crystals lack the real-space inversion symmetry.

We now move on to the nontrivial spin groups. While the above spin-only group is common to all nonrelativistic collinear magnets, we derive three different types of the nontrivial spin groups corresponding, respectively, to the three distinct phases. The nontrivial spin groups are obtained by combining groups of spin-space transformations with groups of real-space crystallographic transformations [24,25]. Regarding the groups of spin-space transformations, there can be some freedom in their choice [24,25]. For the collinear spin arrangements, one of the two spin-space transformation groups is $\mathbf{S}_1 = \{E\}$; i.e., it contains just the spin-space identity [24]. We choose the second group in the form of $\mathbf{S}_2 = \{E, C_2\}$ which is favorable for our derivation of the categorization into the three phases of nonrelativistic collinear magnets. The group contains the spin-space identity and the 180° rotation of the spin space around an axis perpendicular to the spins. (We note that because of the above spin-only group symmetry element \bar{C}_2 , and because the product of spin-space transformations $\bar{C}_2 C_2$ is equal to the spin-space inversion, an alternative choice [24] of \mathbf{S}_2 contains the spin-space inversion instead of C_2 .)

After introducing the spin-only group and the spin-space transformations in the nontrivial spin groups, we move on to the real-space crystallographic transformations in the nontrivial spin groups. The procedure of constructing the nontrivial spin groups applies equally when considering crystallographic space groups (i.e., those containing also translations) or crystallographic point groups (i.e., those where the translations are replaced by identity). To categorize

the nonrelativistic collinear magnets based on their magnetic crystal structure, we need to consider the crystallographic space groups. However, to make our manuscript concise, we do not explicitly list all nontrivial spin groups constructed from the crystallographic space groups. This is because the physical consequence of the third phase that we focus on in this work is the spin-momentum locking in the nonrelativistic band structure. In other words, we focus on determining which momenta in the Brillouin zone have spin-degenerate eigenstates protected by the spin-group symmetries, and for which momenta the spin-group symmetries allow for lifting the spin degeneracy. For all collinear spin arrangements on crystal independent of the crystal's real-space translation symmetries, and independent of whether the crystal does or does not have the real-space inversion symmetry, the spin-momentum locking is described by the direct product of the spin-only group and nontrivial spin groups constructed from the crystallographic point groups containing the real-space inversion symmetry (crystallographic Laue groups).

The general independence of the spin-momentum locking of translations is a consequence of the strict separation of the nonrelativistic band structure into nonmixing spin-up and spin-down channels protected by the spin-only group symmetries of the collinear magnets. The separate spin-up and spin-down channels then have equal energies at a given momentum \mathbf{k} in the Brillouin zone when the nontrivial spin group contains a symmetry element $[C_2|R]$, where R transforms the momentum \mathbf{k} on itself or a momentum separated from \mathbf{k} by a reciprocal lattice vector (R belongs to the little group of \mathbf{k}). Since \mathbf{k} is invariant under translations, the spin degeneracy at a given momentum \mathbf{k} is protected by $[C_2|R]$ irrespective of whether R does or does not contain a translation. Note that additional band degeneracies can exist within one spin channel, i.e., degeneracies in band indices other than spin that are protected by crystallographic space-group symmetries. These features, whose systematic study is beyond the scope of our present manuscript, can be readily included in the symmetry analysis based on the nonrelativistic spin-group formalism and can be important when, e.g., exploring exotic (topological) quasi-particles near such degeneracy points [42–45].

The general invariance of bands of nonrelativistic collinear magnets under real-space (crystal-momentum) inversion is derived above from the spin-only group symmetry $[\bar{C}_2|\mathcal{T}]$. Later in the text, we give specific examples of the inversion-symmetric spin-momentum locking in the band structures of the third phase in crystals with or without the inversion symmetry.

By using the isomorphism theorem [24], we construct all the nontrivial spin (Laue) groups, whose elements on the left of the double vertical bar form a group of the spin-space transformations and on the right of the double vertical bar a (Laue) group of the real-space crystallographic transformations. It implies the procedure of combining all isomorphic coset decompositions of the two groups,

i.e., decompositions with the same number of cosets for the two groups [24]. (A coset decomposition of a group \mathbf{X} is given by $\mathbf{X} = \mathbf{x} + X_1\mathbf{x} + X_2\mathbf{x} + \dots$, where \mathbf{x} is a subgroup of \mathbf{X} , and X_i are elements of \mathbf{X} [24].) The details of our derivation are in the Supplemental Material Sec. II [30]. Here we summarize the result in which all the nontrivial spin Laue groups describing $\epsilon(s, \mathbf{k})$ of collinear magnets are arranged into the following three distinct types using the isomorphic coset decompositions.

The first type of nontrivial spin Laue group is given by $\mathbf{R}_s^I = [E||\mathbf{G}]$, where \mathbf{G} are the crystallographic Laue groups. Because there are 11 different crystallographic Laue groups, there are also 11 different \mathbf{R}_s^I groups. As highlighted in Fig. 1, the \mathbf{R}_s^I groups do not imply spin degeneracy of $\epsilon(s, \mathbf{k})$ at any \mathbf{k} -point. They describe nonrelativistic spin-split band structures with broken time-reversal symmetry and nonzero magnetization corresponding to conventional collinear ferromagnets (ferrimagnets) whose magnetic crystal structure contains one spin lattice (or the opposite-spin sublattices are not connected by any spin-space-group transformation).

The second type of nontrivial spin Laue group is given by $\mathbf{R}_s^{II} = [E||\mathbf{G}] + [C_2||\mathbf{G}]$. Here, the $[C_2||E]$ symmetry (recall that \mathbf{G} is a group containing the real-space identity E element) implies spin degeneracy of $\epsilon(s, \mathbf{k})$ for all \mathbf{k} -vectors in the Brillouin zone. The 11 different \mathbf{R}_s^{II} groups describe nonrelativistic spin-degenerate time-reversal invariant band structures with zero magnetization of conventional collinear antiferromagnets (see Fig. 1). The corresponding antiferromagnetic spin arrangements on crystals have a symmetry $[C_2||\mathbf{t}]$ in their spin-space group, which interchanges atoms and rotates the spin by 180° between opposite-spin sublattices. Here, \mathbf{t} on the right side of the double vertical bar is a real-space translation. Examples [62,63] are antiferromagnets FeRh or MnBi_2Te_4 . The \mathbf{R}_s^{II} groups also describe nonrelativistic spin-degenerate collinear antiferromagnetism in crystals with the opposite-spin-sublattice transformation symmetry $[C_2||\bar{E}]$, where \bar{E} on the right side of the double vertical bar is the real-space inversion. This is because of the spin-only group symmetry $[\bar{C}_2||T]$ that implies the inversion symmetry of the bands, i.e., that the bands in all nonrelativistic collinear magnets are

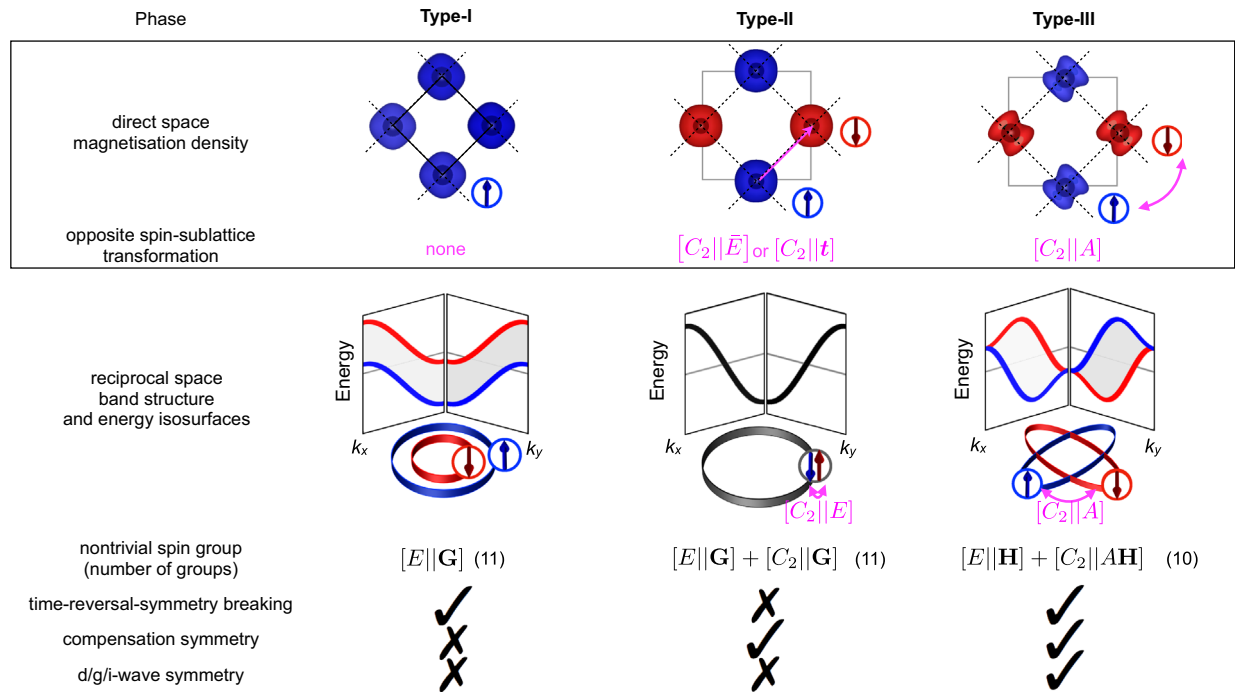


FIG. 1. Illustration (in columns) of the three nonrelativistic collinear magnetic phases. Top box: Illustrative collinear spin arrangements and magnetization densities on crystals. Opposite spin directions are depicted by blue and red color. Spin arrows are placed outside the real-space cartoons to highlight that the overall spin axis orientation is not related to the real space coordinates for the nonrelativistic spin-group symmetries. 1st magnetic phase (conventional ferromagnetism) crystal corresponds to Fe, 2nd magnetic phase (conventional antiferromagnetism) to MnPt, and the 3rd unconventional magnetic phase (altermagnetism) to RuO_2 . Magenta arrow and magenta label highlight opposite-spin-sublattice transformation characteristic of the 2nd magnetic phase (real-space translation or inversion) and the 3rd magnetic phase (real-space rotation). Bottom box: Cartoons of band-structures and corresponding energy iso-surfaces show ferromagnetically spin-split bands (opposite spin states depicted by blue and red color), a spin-degenerate antiferromagnetic band, and bands in the 3rd magnetic phase with alternating sign of the spin splitting. The opposite-spinsublattice transformation of the spin Laue group which maps the same-energy eigenstates with opposite spins on the same \mathbf{k} -vector in the 2nd magnetic phase and on different \mathbf{k} -vectors in the 3rd magnetic phase is again highlighted. The remaining rows give the spin Laue group structure for the given phase with the number of different groups in brackets, and presence/absence of time-reversal-symmetry breaking, compensation and d -, g -, and i -wave symmetries.

invariant under the transformation $[E||\bar{E}]$. Symmetries $[C_2||\bar{E}]$ and $[E||\bar{E}]$ give the $[C_2||E]$ symmetry that implies the spin degeneracy across the Brillouin zone (for a more detailed derivation, see Supplemental Material Sec. II [30]). Here, the examples [50,64] are antiferromagnets CuMnAs or Mn₂Au.

The remaining third distinct type of nontrivial spin Laue group describes the third magnetic phase and is given by

$$\mathbf{R}_s^{\text{III}} = [E||\mathbf{H}] + [C_2||A][E||\mathbf{H}] = [E||\mathbf{H}] + [C_2||\mathbf{G} - \mathbf{H}]. \quad (1)$$

Here, \mathbf{H} is a halving subgroup of the crystallographic Laue group \mathbf{G} and the coset $\mathbf{G} - \mathbf{H} = A\mathbf{H}$ is generated by transformations A that can be only real-space proper or improper rotations and cannot be real-space inversion. (Note that this implies that the real-space inversion that is always present in \mathbf{G} is contained in \mathbf{H} .) We see from Eq. (1) that for $\mathbf{R}_s^{\text{III}}$, \mathbf{G} is expressed as a sublattice coset decomposition, where the halving subgroup \mathbf{H} contains only the real-space transformations which interchange atoms between same-spin sublattices, and the coset $\mathbf{G} - \mathbf{H}$ contains only the real-space transformations which interchange atoms between opposite-spin sublattices. The third magnetic phase corresponds to the magnetic crystal structures in which opposite-spin sublattices are connected by rotation (proper or improper and symmorphic or nonsymmorphic) and are not connected by translation or inversion.

The third-phase magnets have nonrelativistic spin-split band structures with broken time-reversal symmetry and zero magnetization [1] (see Fig. 1). The broken time-reversal symmetry is seen when multiplying $[C_2||\mathbf{G} - \mathbf{H}]$ by the spin-only group symmetry $[\bar{C}_2||T]$, which gives $[\bar{E}||T(\mathbf{G} - \mathbf{H})]$ [or equivalently, $[T||T(\mathbf{G} - \mathbf{H})]$]; i.e., spin groups of the third type do not contain the time-reversal symmetry element. (Recall that the coset $\mathbf{G} - \mathbf{H}$ does not contain the identity element.) Lifted spin degeneracies in the $\mathbf{R}_s^{\text{III}}$ groups are allowed for crystal momenta whose little group does not contain $A\mathbf{H}$ elements. They satisfy $A\mathbf{H}\mathbf{k} = \mathbf{k}' \neq \mathbf{k}$, implying that $\epsilon(s, \mathbf{k}) = [C_2||A\mathbf{H}]\epsilon(s, \mathbf{k}) = \epsilon(-s, \mathbf{k}')$ (see Fig. 1). It guarantees that the spin-up and spin-down energy isosurfaces are split, but have the same number of states. These nonrelativistic band-structure signatures of the $\mathbf{R}_s^{\text{III}}$ phase are unparalleled in the \mathbf{R}_s^{I} or \mathbf{R}_s^{II} phases. Simultaneously, there are ten different $\mathbf{R}_s^{\text{III}}$ groups which is comparable to the number of \mathbf{R}_s^{I} or \mathbf{R}_s^{II} groups, suggesting that the third phase is abundant. The ten nontrivial spin Laue groups of the third phase are listed in Fig. 2, where we adopt Litvin's notation of the spin groups [25], with the upper index 1 refers to the spin-space identity and the upper index 2 to the spin-space rotation C_2 . Note that they are constructed from only eight different crystallographic Laue groups. However, the third-phase spin Laue groups cannot be constructed for the three remaining crystallographic

Laue groups, namely, from $\mathbf{G} = \bar{1}$, $\bar{3}$, or $m\bar{3}$. In the Supplemental Material Sec. II Table S1 [30], we list all 37 nontrivial spin point groups of the third magnetic phase, together with their corresponding ten nontrivial spin Laue groups.

Before moving to the analysis of the spin-momentum locking protected by the symmetries of the third-phase spin groups, we emphasize the additional differences from the magnetic groups. The latter are constructed by combining crystallographic groups (with the same transformations acting simultaneously on coordinates of atoms and components of magnetic moment vectors) with one group containing the identity element alone, and a second group containing the identity and the time reversal. Comparing this construction to the spin-group formalism with \mathbf{S}_1 also containing only the identity element and \mathbf{S}_2 with again two elements, implies that for describing all magnetic structures, the relativistic symmetry formalism has the same number of different magnetic groups as is the number of different nonrelativistic spin groups describing exclusively collinear spin arrangements. For the Laue (point) groups, the total number is 32 (122). Our nonrelativistic spin groups then split into 11 (32) nontrivial spin Laue (point) groups of the ferromagnetic phase, 11 (53) of the antiferromagnetic phase, and ten (37) of the third magnetic phase (see Supplemental Material Sec. II Table S1 [30]).

We also note that because of the crystallographic operations applied in the coupled real and spin space, there is no counterpart in the magnetic groups of the sublattice coset decomposition form of the $\mathbf{R}_s^{\text{III}}$ spin groups (see Supplemental Material Sec. II [30]). As we further highlight below, the decomposition into same-spin- and opposite-spin-sublattice transformations in $\mathbf{R}_s^{\text{III}}$ plays a central role in understanding the third magnetic phase.

III. SPIN-MOMENTUM LOCKING PROTECTED BY SPIN SYMMETRIES

We now discuss the basic characteristics of the spin-momentum locking in the third magnetic phase as derived from the spin Laue group symmetries, i.e., from the symmetries of the direct product of the spin-only group and the nontrivial spin Laue groups. We derive above that the nonrelativistic collinear magnetic order described by the spin-only group symmetries implies that spin is a good quantum number with a common \mathbf{k} -independent quantization axis, and that the bands are space-inversion symmetric (symmetric with respect to the inversion of \mathbf{k}). We also derive that the bands in the third phase described by the nontrivial spin Laue groups $\mathbf{R}_s^{\text{III}}$ break the time-reversal symmetry. The space-inversion symmetry implies that the bands are even in momentum around the Γ -point. Moreover, the Γ -point is invariant under all real-space transformations. The $[C_2||A]$ symmetry present in the $\mathbf{R}_s^{\text{III}}$ groups thus guarantees spin degeneracy of the Γ -point.


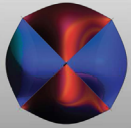
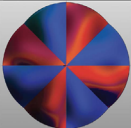
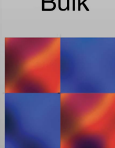
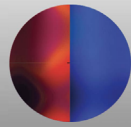
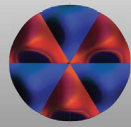
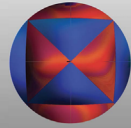
Spin-momentum locking			\mathbf{G}	$\mathbf{R}_s^{\text{III}}$	\mathbf{H}	\mathbf{A}	Candidate
Planar  (k_x, k_y)	P-2 <i>d</i> -wave 	(k_x, k_y)	mmm	${}^2m^2m^1m$ (8)	$2/m$	C_{2x}	La ₂ CuO ₄ , FeSb ₂
			$4/m$	${}^24/1^1m$ (8)		C_{4z}	KRu ₄ O ₈
	P-4 <i>g</i> -wave 	(k_x, k_y)	$4/mmm$	${}^{24/1}m^2m^1m$ (16)	$4/m$	C_{4z}	RuO ₂ , MnO ₂ , MnF ₂
${}^{14/1}m^2m^2m$ (16)				C_{2x}		KMnF ₃	
Bulk  (k_x, k_y, k_z)	B-2 <i>d</i> -wave 		$2/m$	${}^22/2^2m$ (4)	$\bar{1}$	C_{2z}	CuF ₂
	B-4 <i>g</i> -wave 		$\bar{3}m$	${}^{1\bar{3}2}m$ (12)	$\bar{3}$	C_{21}	CoF ₃ , FeF ₃ , Fe ₂ O ₃
			$6/m$	${}^{26/2}m$ (12)		C_{6z}	
	B-6 <i>i</i> -wave 		$6/mmm$	${}^{26/2}m^2m^1m$ (24)	$\bar{3}m$	C_{6z}	CrSb, MnTe, VNb ₃ S ₆
			$m\bar{3}m$	${}^1m^1\bar{3}^2m$ (48)	$m\bar{3}$	C_{4z}	

FIG. 2. Classification of spin-momentum locking in the third magnetic phase protected by spin-group symmetries, and material candidates. The columns describe the characteristic planar (P) or bulk (B) spin-momentum locking on model Hamiltonian bands with the characteristic spin-group integer and the even-parity wave form of altermagnetism, the crystallographic Laue group \mathbf{G} , the halving subgroup \mathbf{H} of symmetry elements which interchange atoms between same-spin sublattices, a generator A of symmetry elements which interchange atoms between opposite-spin sublattices, the nontrivial spin Laue group $\mathbf{R}_s^{\text{III}}$ (in brackets we list the number of symmetry elements), and material candidates of the third magnetic phase. The model Hamiltonian bands on which we illustrate the spin-momentum locking character are described in Supplemental Material Sec. III [30]. References describing the materials are in the main text and Supplemental Material Secs. V–VI [30].

On the other hand, lifted spin degeneracies in the rest of the Brillouin zone, including other time-reversal invariant momenta, are not generally excluded in the third phase.

These basic spin-momentum locking characteristics of the third phase are in striking contrast to the spin-momentum locking in crystals with Kramers spin degeneracy lifted by the relativistic spin-orbit coupling. The relativistic spin-momentum locking has the form of a continuously varying spin texture in the momentum space, it is not symmetric with respect to the inversion of \mathbf{k} because of the required broken real-space inversion symmetry of the crystal, the bands are time-reversal invariant, and all time-reversal invariant momenta are spin degenerate. These distinct characteristics of the relativistic

spin-momentum locking apply to nonmagnetic systems [65], as well as to conventional antiferromagnets with broken real-space inversion symmetry and spin-orbit-coupling effects included. An example is the relativistic time-reversal invariant band structure with Rashba spin splitting in a noncentrosymmetric antiferromagnet BiCoO₃ with the opposite-spin sublattices connected by translation [52].

Other prominent spin-momentum locking features in the third phase are protected by the specific $[C_2\|A][E\|\mathbf{H}]$ symmetries present in the given $\mathbf{R}_s^{\text{III}}$ group. For example, a symmetry $[C_2\|M_c]$, where c is the axis perpendicular to the a - b mirror plane, defines a spin-degenerate $k_a - k_b$ nodal plane at $k_c = 0$, or other k_c separated from $M_c k_c = -k_c$ by a reciprocal lattice vector. This is because $[C_2\|M_c]$

transforms a wave vector from this plane on itself, or on an equivalent crystal momentum separated by the reciprocal lattice vector, while spin is reversed. Similarly, a $[C_2||C_{n,c}]$ symmetry, where $C_{n,c}$ is an n -fold rotation symmetry around the c axis, imposes a spin-degenerate nodal line parallel to the k_c axis for wave vectors with $k_a = k_b = 0$, or other $k_{a(b)}$ separated from $C_{n,c}k_{a(b)}$ by a reciprocal lattice vector. We note that the high-symmetry planes or lines are typically of main focus when assessing the electronic structures. This may explain why, apart from the omission by the conventional magnetic groups, the third phase remained unnoticed during the decades of DFT and experimental studies of band structures.

Each of the ten $\mathbf{R}_s^{\text{III}}$ spin Laue groups classifying the spin-momentum locked band structures can be assigned a characteristic even integer, which we define as follows. When making a closed loop in the momentum space around the Γ -point in a plane orthogonal to a spin-degenerate nodal surface crossing the Γ -point, the spin rotates by 360° following two discrete reversals. Each spin-degenerate nodal surface crossing the Γ -point that is present in the crystal momentum space generates such a spin rotation. We define the characteristic spin-group integer as a number of these spin-degenerate nodal surfaces crossing the Γ -point. The spin-group integer is given in Fig. 2, and it is an even number ranging from 2 to 6. As an illustration, we show in the Supplemental Material Sec. III and Fig. S2 [30] spin-degenerate nodal planes crossing the Γ -point corresponding to mirror-symmetry planes combined with spin-space rotation for representative $\mathbf{R}_s^{\text{III}}$ groups from Fig. 2.

In Fig. 2, we show the characteristic spin-group integer next to a spin-momentum locking depicted on top of model Hamiltonian bands. The six model Hamiltonians, with anisotropic d -wave, g -wave, and i -wave harmonic symmetry are listed in Supplemental Material Sec. III [30] and are derived to have the same spin-degenerate nodal planes crossing the Γ -point as the nodal planes corresponding to the representative $\mathbf{R}_s^{\text{III}}$ groups in Supplemental Material Fig. S2 [30]. We obtain either planar or bulk nonrelativistic spin-momentum locking, with the characteristic spin-group integer from 2 to 6. The planar spin-momentum locking is relevant for (quasi)two-dimensional and three-dimensional crystals, while the bulk spin-momentum locking only for three-dimensional crystals. We note that the earlier reported materials [1,2,4–11,16–22,66–68] FeF_2 , MnO_2 , RuO_2 , $\kappa\text{-Cl}$, MnF_2 , Mn_5Si_3 , LaMnO_3 , FeSb_2 , and CaCrO_3 referred to as unconventional spin-split antiferromagnets in these studies, all correspond to the third magnetic phase with the characteristic planar spin-momentum locking and spin-group integer 2.

The presence of nonrelativistic anisotropic spin-dependent conductivities in the third-phase magnets and the corresponding giant-magnetoresistance and spin-torque phenomena [16,17] is symmetrywise more restrictive than the presence of the phase itself [17]. Only the $\mathbf{R}_s^{\text{III}}$ spin

Laue groups with the characteristic spin-group integer 2 ($\mathbf{R}_s^{\text{III}} = {}^2m^2m^1m$, ${}^{24/1}m$, ${}^{24/1}m^2m^1m$, and ${}^{22/2}m$) have a sufficiently low symmetry that allows for these prominent time-reversal symmetry-breaking spintronic effects in the third magnetic phase.

IV. SPIN SPLITTING BY THE ELECTRIC CRYSTAL POTENTIAL

In Supplemental Material Sec. IV [30], we summarize the properties of the third magnetic phase derived from the spin Laue group symmetries. Among those, we highlight here the symmetry principles which guide us to the discovery of an extraordinary spin-splitting mechanism, which we illustrate on KRu_4O_8 and RuO_2 . The latter example, in which the amplitude of the extraordinary spin splitting is on the eV scale, is the workhorse material in the emerging research field of time-reversal symmetry-breaking spintronic phenomena in the third magnetic phase [1,3,16–18,20–22].

The spin-symmetry guiding principles for the extraordinary spin splitting by the electric crystal potential are as follows: (i) The magnetic crystals should be anisotropic to allow for the symmetries defining the third magnetic phase $[C_2||\mathbf{G} - \mathbf{H}]$, which separate opposite-spin equal-energy states in the momentum space. (ii) The symmetries interchanging atoms within the same-spin sublattice $[E||\mathbf{H}]$ should be low enough to generate a sufficient anisotropy in the momentum space of the bands dominated by the given sublattice. (iii) The symmetries of \mathbf{G} are high enough to allow for the orbital degeneracy at the Γ -point; this is fulfilled in all groups \mathbf{G} allowing for the third magnetic phase, except for $\mathbf{G} = mmm$ or $2/m$. (iv) The chemistry should allow for these degenerate orbitals to be present in the material and in the desired part of the energy spectrum (e.g., near the Fermi level).

We first illustrate how these principles for identifying outlier spin splittings materialize in a pristine way in ruthenate KRu_4O_8 when hosting the third magnetic phase. The signature of the extraordinary microscopic spin-splitting mechanism is that its size and momentum dependence are determined by the electric crystal potential of the nonmagnetic phase. The material fulfills all the above spin-symmetry guiding principles, including its corresponding $\mathbf{G} = 4/m$. (In contrast, LaMnO_3 , $\kappa\text{-Cl}$, FeSb_2 , or CaCrO_3 have $\mathbf{G} = mmm$ [2,6,10,11,68] that excludes this electric-crystal-potential mechanism of the spin splitting.)

The real-space crystal structure of KRu_4O_8 , as reported in earlier studies [69,70], is schematically illustrated in Fig. 3(a). The symmetry of the lattice is body-centered tetragonal (crystallographic space group $I4/m$). Red and blue color in Fig. 3(a) represent the collinear antiparallel spin arrangement on the crystal. In addition, the A and B symbols label the real-space sublattices corresponding to the opposite spins in the third magnetic phase. The A and B real-space sublattices are strongly anisotropic and related

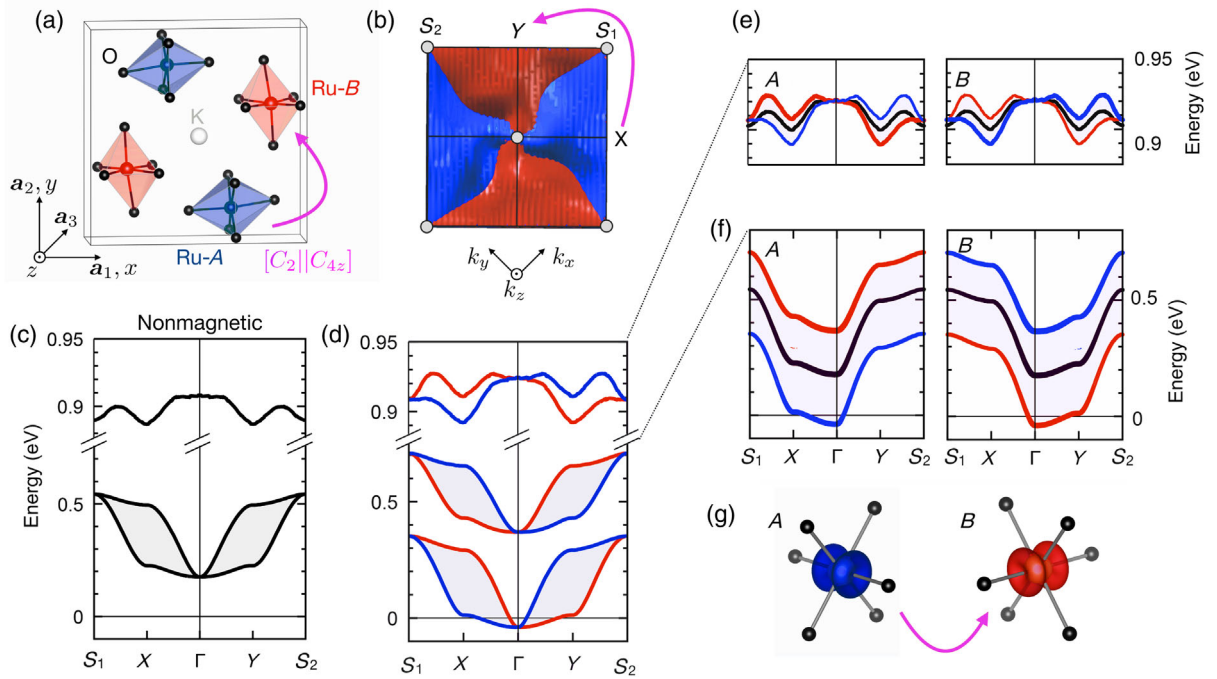


FIG. 3. Spin splitting by the electric crystal potential in KRu_4O_8 in the third magnetic phase. (a) Schematic spin arrangement on the KRu_4O_8 crystal with opposite-spin directions depicted by red and blue color. Magenta arrow and its label highlights the opposite-spin-sublattice transformation containing a real-space fourfold rotation. (b) Calculated spin-momentum locking with the characteristic spin-group integer 2 on top of two DFT Fermi surface sheets. (c),(d) DFT band structure of the nonmagnetic phase and the third magnetic phase, respectively. Gray shading highlights the \mathbf{k} -dependent splitting by the anisotropic electric crystal potential. (e),(f) Projection of bands on the sublattices A and B in the nonmagnetic phase (black) and third magnetic phase (red and blue) for the upper bands and lower bands, respectively. Color shading in (f) highlights the nearly \mathbf{k} -independent magnetic splitting of the lower bands, and its opposite sign for the sublattices A and B bands. (g) Real-space DFT spin density around the Ru atom in sublattices A and B .

by a mutual planar rotation by 90° (C_{4z}). Correspondingly, the nontrivial spin Laue group describing the spin-momentum locking in the third magnetic phase is ${}^2_4/m$. According to Eq. (1), it can be decomposed as

$${}^2_4/m = [E||2/m] + [C_2||C_{4z}][E||2/m]. \quad (2)$$

Figure 3(b) shows the DFT calculation of the spin-momentum locking protected by the spin-group symmetries, on top of two selected KRu_4O_8 Fermi surface sheets. (The band structure is obtained using the DFT full-potential linearized augmented-plane-wave code ELK within the local-spin-density generalized-gradient approximation [71].) In particular, the $[C_2||C_{4z}]$ symmetry leads to three spin-degenerate nodal lines parallel to the k_z axis, $[0, 0, k_z]$, $[2, 0, k_z]$, and $[0, 2, k_z]$ marked by gray points in Fig. 3(b) (here the wave vectors are in units of π divided by the lattice constant). The latter two correspond, for $k_z = 0$, to time-reversal invariant momenta S_1 and S_2 . On the other hand, the spin degeneracy is strongly lifted at time-reversal invariant momenta X and Y corresponding to the directions of the real-space anisotropy axes of the two sublattices. Consistently, the little crystallographic Laue group at the X and Y wave vectors is $2/m$, which coincides with the

halving subgroup of same-spin-sublattice transformations. The spin-momentum locking is planar, reflecting the real-space planar mutual rotations of the crystal anisotropies of the opposite-spin sublattices, and the characteristic spin-group integer is 2.

We now move on to the demonstration of the spin splitting whose size and momentum dependence are determined by the electric crystal potential and compare this extraordinary microscopic mechanism to the more conventional magnetic spin-splitting mechanism. The analysis is presented in Figs. 3(c)–3(g). Energy bands in the nonmagnetic and third magnetic phase are shown in Figs. 3(c) and 3(d). The high-energy band around 0.9 eV in the depicted portion of the Brillouin zone is twofold spin degenerate in the nonmagnetic phase [upper part of Fig. 3(c)]. The magnetic component of the internal electromagnetic crystal potential in the magnetic phase generates an anisotropic \mathbf{k} -dependent spin splitting, as shown in the upper part of Fig. 3(d) where the red and blue color correspond to opposite spin states. The sign of the spin splitting alternates, following the symmetries of the spin group. This type of spin splitting belongs to a family generally referred to as internal magnetic-interaction mechanisms [4,7,8,17].

The other bands of KRu_4O_8 for energies near the Fermi level also show a spin splitting within the DFT band-structure theory. However, here the microscopic origin is fundamentally distinct from the internal magnetic-interaction mechanisms. In the nonmagnetic phase, we observe in the lower part of Fig. 3(c) a couple of twofold spin-degenerate bands whose mutual splitting (highlighted by gray shading) by the electric crystal potential is \mathbf{k} dependent, merging at the fourfold degenerate Γ , S_1 , and S_2 points. Remarkably, the \mathbf{k} -dependent spin splitting in the magnetic phase in the lower part of Fig. 3(d) (highlighted again by gray shading) copies the size and \mathbf{k} dependence of the band splitting by the electric crystal potential of the nonmagnetic phase. Its microscopic explanation is provided in Figs. 3(f) and 3(g).

We start the discussion of Fig. 3(f) from the projections of the bands on the sublattices A and B in the nonmagnetic phase (black lines). The projections are dominated by Ru d_{xz} and d_{yz} orbitals. This is in agreement with earlier report [70], which showed the presence of Ru t_{2g} orbitals near the Fermi level. At the Γ -point, the A and B projected bands are degenerate, which is consistent with the octahedral environment with the tetragonal symmetry [72]. Including spin, the Γ -point is then fourfold degenerate in the nonmagnetic phase.

The band whose dominant weight is on sublattice A is strongly anisotropic with respect to \mathbf{k} when moving toward the X and Y points [left panel of Fig. 3(f)]. The same applies to the sublattice B band; however, the sense of the anisotropy reverses [right panel of Fig. 3(f)]. The band anisotropies reflect the strong crystalline anisotropy, conspiring with the favorable symmetry of the involved orbitals. By adding up the A and B projections, we obtain the bands shown in Fig. 3(c). They progressively split by the electric crystal potential when the \mathbf{k} -vector moves from the Γ -point toward, e.g., the X point, with the lower band dominated by one sublattice and the upper band by the other sublattice. Along the $\Gamma - \text{Y}$ line, the sublattice indices of the lower and upper bands switch places.

The bands in the magnetic phase projected again on sublattices A and B are also plotted in Fig. 3(f). As in Fig. 3(d), the red and blue colors correspond to opposite spins. We see that for bands with dominant weight on sublattice A , spin states shown in red move up in energy, while the opposite spin states shown in blue move down [left panel of Fig. 3(f)]. The magnetic component of the internal crystal potential in the magnetic phase generates in this case a splitting (highlighted by light-blue shading), which is nearly \mathbf{k} independent. This scenario is fundamentally distinct from the strongly \mathbf{k} -dependent magnetic splitting of the high-energy band shown in Fig. 3(e). It is reminiscent of ferromagnets. However, unlike the common ferromagnetic case, the nearly \mathbf{k} -independent magnetic splitting reverses sign for the sublattice B bands [right panel of Fig. 3(f)]. This locality, in which band states near

the Fermi level with one spin have a dominant weight on one sublattice, is again distinct from the delocalized nature of spin states in the high-energy bands shown in Fig. 3(e). It also starkly contrasts with the conventional mechanisms of the ferromagnetic splitting of band spin states experiencing the global magnetization or the relativistic spin-orbit splitting due to the global electric inversion asymmetry. An additional illustration of the locality is shown in Fig. 3(g) where we plot the real-space DFT spin density around the Ru atom in sublattices A and B . Consistent with the spin-group symmetry and the dominant d_{xz} and d_{yz} orbitals near the Fermi level, the opposite-spin local densities in the two sublattices are highly anisotropic with the mutually rotated real-space anisotropy axes.

Adding up the A and B sublattice projections of Fig. 3(f) then explains the formation of two pairs of spin-split bands seen in Fig. 3(d). The mutual magnetic splitting between the two pairs is nearly \mathbf{k} independent, while the spin splitting within each pair is a \mathbf{k} -dependent copy of the band splitting by the anisotropic electric crystal potential of the nonmagnetic phase [Fig. 3(c)]. It also explains that the two pairs have opposite sign of the spin splitting and that, within each pair, the spin-splitting sign is opposite when moving from the Γ -point toward the X or Y points. We see from Figs. 3(d) and 3(f) that even if the nearly \mathbf{k} -independent magnetic splitting were small, the electric crystal potential of the nonmagnetic phase would still determine the splitting between the two nearest bands with opposite spin in the magnetic phase at \mathbf{k} -vectors sufficiently close to the Γ -point. This is a consequence of the nearly \mathbf{k} -independent magnetic band splitting and of the spin degeneracy of the Γ -point in the third magnetic phase.

In the studied KRu_4O_8 , the spin splitting originating from this extraordinary electric-crystal-potential mechanism reaches a 300-meV scale. In Supplemental Material Sec. V and Fig. S3 [30], we show that in RuO_2 , a spin splitting reaching a 1-eV scale [1,4,17] is also due to the electric-crystal-potential mechanism. These spin-splitting magnitudes are comparable to spin splittings in ferromagnets but, unlike ferromagnets, are accompanied by a zero net magnetization. They also illustrate that spin splittings in the third magnetic phase can exceed by an order of magnitude the record relativistic spin-orbit splittings in bulk crystals with heavy elements [73]. Moreover, unlike the spin-orbit split bands, the third magnetic phase preserves a common \mathbf{k} -independent spin quantization axis.

Finally, we emphasize that relativistic DFT calculations in RuO_2 and KRu_4O_8 presented in Supplemental Material Sec. V and Figs. S3 and S4 [30] show the expected weak effect of the spin-orbit coupling on the bands. This highlights that the apparent prominent features of the relativistic bands, including the spin-momentum locking characteristics and the electric-crystal-potential mechanism of the spin splitting, still reflect the nonrelativistic spin-group

symmetries. In contrast, these prominent symmetries are omitted by the relativistic magnetic groups of RuO_2 and KRu_4O_8 . In general, as also illustrated in Supplemental Material Secs. III and IV and Figs. S3 and S4 [30], only the spin-group formalism facilitates the sublattice coset decomposition into transformations which interchange atoms between same-spin and opposite-spin sublattices, which plays the central role in understanding the third magnetic phase. Apart from the spin-symmetry guiding principles and DFT calculations of the spin splitting by the electric crystal potential, we also provide a description of this extraordinary mechanism by a minimal lattice model in Supplemental Material Sec. V Fig. S5 [30].

V. CANDIDATE MATERIALS

Figure 2 lists the selected candidate materials for the third magnetic phase. In Fig. 4, we highlight CrSb, a metal with the critical temperature of 705 K [74]. As shown in Fig. 4(a), it crystallizes in the hexagonal NiAs-type structure (crystal space group $P6_3/mmc$) [74,75]. The collinear antiparallel spin arrangement corresponds to the nontrivial spin Laue group ${}^2_6/2m^2m^1m$ ($[E||\bar{3}m] + [C_2||C_{6z}][E||\bar{3}m]$). It contains the $[C_2||M_z]$ symmetry, which makes the spin-momentum locking bulklike. Additional mirror planes orthogonal to the three hexagonal crystal axes combined with the spin rotation imply that the characteristic spin-group integer is 4 (see Supplemental

Material Fig. S2 [30]). This is confirmed by the DFT calculations in Fig. 4(b).

CrSb has a more complex band structure than KRu_4O_8 , as shown in Fig. 4(c). Nevertheless, we can trace a pair of bands with opposite spin [highlighted by gray shading in Fig. 4(c)] which are degenerate at the Γ , L_1 , and L_2 points and split when moving away from these high-symmetry points. The spin splitting is as high as 1.2 eV. We also note that CrSb hosts an exotic spin-polarized quasiparticle which is fourfold degenerate at the Γ -point and spin split away from the Γ -point.

A semiconducting MnTe, which is isostructural to CrSb, also hosts an extraordinarily large spin splitting in the valence band of 1.1 eV. In Supplemental Material Sec. V Fig. S6 [30], we give a summary of the spin splittings vs critical temperature in selected materials hosting the third magnetic phase. In Supplemental Material Sec. VI and Figs. S7 and S8 [30], we discuss additional material candidates among insulators, semiconductors, and metals, and give an example illustrating the inversion symmetry of the nonrelativistic bands of the third magnetic phase even when the crystal is inversion asymmetric (VNb_3S_6).

Finally, we discuss the parent cuprate La_2CuO_4 of a high-temperature superconductor [27,76]. The band structure for the collinear antiparallel spin arrangement on this crystal falls into the $\mathbf{R}_s^{\text{III}}$ nontrivial spin Laue group ${}^2m^2m^1m$ ($[E||2/m] + [C_2||C_{2y}][E||2/m]$). The symmetry element $[C_2||C_{2y}]$ generates a planar spin-momentum locking

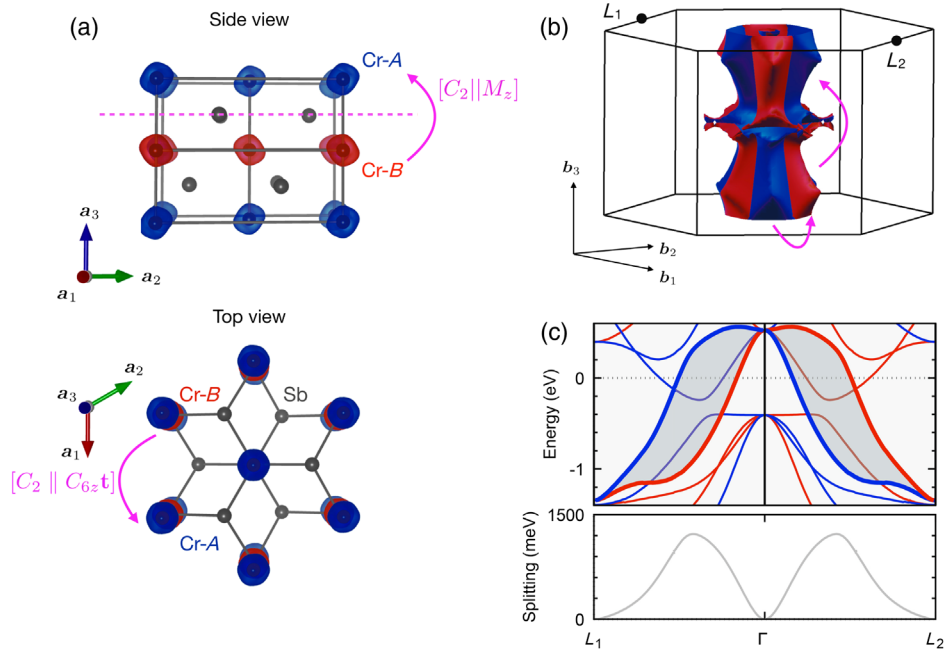


FIG. 4. Metallic high critical temperature CrSb with the third magnetic phase. (a) Schematic crystal structure with DFT spin densities. Cr sublattices and the respective magnetization densities with opposite orientation of the magnetic moment are depicted by red and blue color. Magenta arrow and its label highlights the opposite-spin-sublattice transformation containing a real-space mirror or sixfold rotation. (b) Calculated bulklike spin-momentum locking with the characteristic spin-group integer 4 on top of two selected DFT Fermi surface sheets. (c) DFT band structure in the third magnetic phase. Wave-vector dependence of the spin splitting between the bands highlighted by the gray shading is plotted in the lower panel.

with the characteristic spin-group integer 2. Remarkably, according to our symmetry analysis based on the spin-group theory, the energy bands of La_2CuO_4 are spin split and break time-reversal symmetry. This is confirmed by the DFT calculations in Supplemental Material Fig. S9 [30] and is in contrast with the conventional perception of spin-degenerate bands in La_2CuO_4 [76]. The omission of the spin-splitting physics in earlier electronic-structure studies of cuprates could be explained by the focus on high-symmetry lines or planes, such as the $k_z = 0$ plane [61], where the states are spin degenerate (see Supplemental Material Fig. S9 [30]).

VI. BROAD RELEVANCE IN CONDENSED-MATTER PHYSICS

Our spin-group delimitation and description of the third magnetic phase and the discovery of the extraordinary spin-splitting mechanism by the electric crystal potential in the Ru-oxide crystals provides a unifying theory picture of recent intriguing theoretical and experimental observations of broken time-reversal symmetry transport anomalies and spintronic effects in the magnetically compensated RuO_2 . These include the large crystal (anomalous) Hall effect, charge-spin conversion and spin-torque phenomena, and giant and tunneling magnetoresistance [1,3,16–22]. Our identification of the third magnetic phase in chalcogenide CoNb_3S_6 , perovskite CaMnO_3 , or cuprate La_2CuO_4 also sheds new light on puzzling time-reversal breaking magnetotransport anomalies reported in earlier studies of these materials [77–79].

The diversity of the material types illustrates the relevance of the third magnetic phase for a range of condensed-matter physics fields prone to generate new discoveries. Spintronics based on this phase [1,3,6,9,11,12,16–22] would circumvent the traditional prerequisites of magnetization or relativistic spin-orbit coupling in conventional ferromagnetic spintronics [80–83]. Unlike ferromagnets, the third magnetic phase eliminates stray fields and adds insensitivity to external magnetic field perturbations, while allowing for the strong nonrelativistic effects which facilitate the reading and writing functionalities in commercial spintronics. When comparing to the relativistic nonmagnetic spin-texture phases, these textures share with the third magnetic phase the zero net magnetization. However, large relativistic spin splittings require rare heavy elements. In addition, the relativistic phases suffer from spin decoherence even for small-angle elastic scattering off common isotropic impurities. We illustrate that this obstacle is diminished in the third magnetic phase by the collinearity of spins and by the possibility of a large- \mathbf{k} -vector separation in the Brillouin zone of the equal-energy eigenstates with the opposite spin.

Our results on the ruthenate KRu_4O_8 illustrate the distinct features of nonrelativistic valleytronics in the third magnetic phase, in comparison to valleytronics in nonmagnetic 2D materials [84]. Here the specific merit of the

third magnetic phase are spin-split valleys at time-reversal invariant momenta. Both the spintronics and valleytronics fields can take advantage of the spin-conserving nature of the third magnetic phase, stemming from its nonrelativistic origin in the nonfrustrated collinear magnetic crystals.

Unexplored connections might also exist between the third magnetic phase and topological insulators and semimetals. In this context, we point out that, on the one hand, symmetry prohibits a realization of the third magnetic phase in one-dimensional chains; collinear antiferromagnetic spin arrangements on one-dimensional chains have the $[C_2||\bar{E}]$ (and possibly also $[C_2||\mathbf{t}]$) symmetry and, therefore, have spin-degenerate bands. On the other hand, we identify candidates of the third magnetic phase among quasi-one-dimensional, quasi-two-dimensional, and three-dimensional insulators and metals. This opens the possibility of searching for unconventional spin-polarized fermion quasiparticles (cf. CrSb), topological insulators, and topological semimetals, including Chern insulators with the quantized Hall effect in high-temperature systems with vanishing internal or external magnetic dipole.

In the field of electromagnetic multipoles, the zero magnetic dipole of the third magnetic phase opens a new route for realizing magnetic toroidal phases [8,85]. Related to this is the field of Fermi-liquid instabilities [86], where we show that the principally uncorrelated third magnetic phase represents an unprecedented example of an anisotropic (d -wave, g -wave, or i -wave) instability. Certain anisotropic instabilities were expected in the past to arise in correlated systems [4,86]. Our recognition of the d -wave spin-momentum locking in the parent cuprate crystals of high-temperature d -wave superconductors [87] brings a new element into the research of the coexistence and interplay of magnetic and superconducting quantum orders. In addition to bulk systems, intriguing phenomena can be envisaged also in heterostructures in fields such as topological superconductivity [88].

An extensive perspective on how the emerging third magnetic phase can enrich basic condensed-matter physics concepts and have impact on prominent condensed-matter research and application areas is given in Ref. [89].

VII. DISCUSSION: UNCONVENTIONAL MAGNETIC PHASE

A phase of matter is commonly associated with a uniform state of a physical system and is distinguished from other phases by, among others, crystal structure, composition, or type of order (e.g., magnetic). Each phase in a material system generally exhibits a characteristic set of physical properties, and symmetry is among the fundamental guiding principles for identifying the distinct phases of matter and for describing their phenomenology [31,90]. We show in this work that on the basic level of nonrelativistic physics of nonfrustrated (collinear) magnetism, spin-group symmetries in the crystal-structure real

space and electronic-structure momentum space allow, besides the conventional ferromagnetism and antiferromagnetism, for the third distinct magnetically ordered phase. As summarized in Supplemental Material Figs. S10 and S11 [30], the conventional ferromagnetism is characterized by a type of crystal structure and magnetic order with nonzero magnetization allowed by the spin-group symmetry, while the conventional antiferromagnetism is characterized by a different type of crystal structure and magnetic order with zero net magnetization protected by the spin-group symmetry. The key distinction between the nonrelativistic phenomenologies of the two conventional magnetic phases is the spin-split time-reversal symmetry-broken electronic structure and corresponding time-reversal symmetry-breaking responses in ferromagnets contrasting with the spin-degenerate time-reversal symmetric electronic structure and the absence of time-reversal symmetry-breaking responses in antiferromagnets.

The unconventional magnetic phase classified and described in this work has a type of crystal structure and magnetic order that is distinct from the conventional ferromagnets and antiferromagnets. Its zero net magnetization is protected by the spin-group symmetries that, simultaneously, allow for spin-split time-reversal symmetry-broken electronic structure and corresponding time-reversal symmetry-breaking responses. In trying to retain the classification with only the two traditional basic phases of magnetically ordered materials, a conflict arises. Placing emphasis on the phenomenology of the spin-split time-reversal symmetry-broken electronic structure and responses would lead to a notion of unconventional ferromagnetism. In contrast, emphasizing the zero net magnetization would lead to a notion of unconventional antiferromagnetism. Our work provides a resolution of the conflict by delimiting the unconventional magnetic phase of the d -wave (or high even-parity wave) form as a third distinct symmetry type. The alternating spin polarizations in both real-space crystal structure and momentum-space band structure characteristic of this unconventional magnetic phase suggest a term *altermagnetism*.

We note that on the basic level of nonrelativistic spin-group symmetries, *altermagnetism* is delimited as an exclusive separate phase next to the conventional ferromagnetism and antiferromagnetism, while ferrimagnets are a subclass of ferromagnets. Indeed, in general, a distinction between ferrimagnetic crystals characterized by opposite-spin sublattices not connected by any symmetry transformation, and crystals commonly referred to as ferromagnets can be ambiguous. For example, in crystals referred to as ferrimagnets, all magnetic atoms can be the same chemical elements, and the absence of any crystallographic transformation connecting the opposite-spin sublattices then originates from different local symmetries of the sites occupied by magnetic atoms from the opposite-spin sublattices. This can be compared to crystals commonly

regarded as ferromagnets, where the microscopic spin density changes in magnitude and can also change in sign as a function of the spatial coordinate within the crystal unit cell. Whether or not such variations are correlated with individual atomic species does not change the symmetry of the system.

Finally, we point out that *altermagnetism* is a realization of a long-sought-after counterpart in magnetism of unconventional superconductivity [91]. Magnetism and superconductivity were once regarded as the best understood fields in many-body solid-state physics. Moreover, they were connected by a striking analogy: The electron-electron Cooper pairs forming around the Fermi surface and driving the conventional s -wave superconductivity have a counterpart in the majority spin electron—minority spin-hole pairs distributed isotropically around the Fermi surface in the conventional model of (s -wave) ferromagnetism [91]. The discovery of the unconventional d -wave superconductivity not only opened an entirely new research landscape of this many-body phase [87] but also raised a fundamental question of whether and how an unconventional d -wave counterpart could be realized in magnetism [91]. Earlier considerations focused on possible realizations of the unconventional d -wave magnetism due to strong electronic correlations [86,92,93]. In contrast, our identification is directly linked to symmetries of the crystal potential and does not require strongly correlated systems. This makes the *altermagnetic* materials discussed in our work realistic candidates for a robust unconventional d -wave (or higher even-parity wave) magnetism that can host unconventional time-reversal symmetry-breaking responses of comparable strength to the conventional (s -wave) ferromagnets.

ACKNOWLEDGMENTS

We acknowledge fruitful interactions with Igor Mazin, Rafael González-Hernández, Helen Gomonay, and Roser Valentí. This work is supported by Ministry of Education of the Czech Republic Grants No. LNSM-LNSpin and No. LM2018140, the Czech Science Foundation Grant No. 19-28375X, EU Future and Emerging Technologies Open RIA Grant No. 766566, SPIN + X (Grant No. DFG SFB TRR 173) and Elasto-Q-Mat (Grant No. DFG SFB TRR 288). We acknowledge the computing time granted on the supercomputer Mogon at Johannes Gutenberg University Mainz.

-
- [1] L. Šmejkal, R. González-Hernández, T. Jungwirth, and J. Sinova, *Crystal Time-Reversal Symmetry Breaking and Spontaneous Hall Effect in Collinear Antiferromagnets*, *Sci. Adv.* **6**, eaaz8809 (2020).
 - [2] I. I. Mazin, K. Koepernik, M. D. Johannes, R. González-Hernández, and L. Šmejkal, *Prediction of Unconventional*

- Magnetism in Doped FeSb₂*, *Proc. Natl. Acad. Sci. U.S.A.* **118**, e2108924118 (2021).
- [3] L. Šmejkal, A. H. MacDonald, J. Sinova, S. Nakatsuji, and T. Jungwirth, *Anomalous Hall Antiferromagnets*, *Nat. Rev. Mater.* **7**, 482 (2022).
- [4] K.-H. Ahn, A. Hariki, K.-W. Lee, and J. Kuneš, *Antiferromagnetism in RuO₂ as d-Wave Pomeranchuk Instability*, *Phys. Rev. B* **99**, 184432 (2019).
- [5] S. Hayami, Y. Yanagi, and H. Kusunose, *Momentum-Dependent Spin Splitting by Collinear Antiferromagnetic Ordering*, *J. Phys. Soc. Jpn.* **88**, 123702 (2019).
- [6] M. Naka, S. Hayami, H. Kusunose, Y. Yanagi, Y. Motome, and H. Seo, *Spin Current Generation in Organic Antiferromagnets*, *Nat. Commun.* **10**, 4305 (2019).
- [7] L.-D. Yuan, Z. Wang, J.-W. Luo, E. I. Rashba, and A. Zunger, *Giant Momentum-Dependent Spin Splitting in Centrosymmetric Low-Z Antiferromagnets*, *Phys. Rev. B* **102**, 014422 (2020).
- [8] S. Hayami, Y. Yanagi, and H. Kusunose, *Bottom-Up Design of Spin-Split and Reshaped Electronic Band Structures in Antiferromagnets without Spin-Orbit Coupling: Procedure on the Basis of Augmented Multipoles*, *Phys. Rev. B* **102**, 144441 (2020).
- [9] H. Reichlova *et al.*, *Macroscopic Time Reversal Symmetry Breaking Arising from Antiferromagnetic Zeeman Effect*, arXiv:2012.15651v1.
- [10] L.-D. Yuan, Z. Wang, J.-W. Luo, and A. Zunger, *Prediction of Low-Z Collinear and Noncollinear Antiferromagnetic Compounds Having Momentum-Dependent Spin Splitting Even without Spin-Orbit Coupling*, *Phys. Rev. Mater.* **5**, 014409 (2021).
- [11] M. Naka, Y. Motome, and H. Seo, *Perovskite as a Spin Current Generator*, *Phys. Rev. B* **103**, 125114 (2021).
- [12] H.-Y. Ma, M. Hu, N. Li, J. Liu, W. Yao, J.-F. Jia, and J. Liu, *Multifunctional Antiferromagnetic Materials with Giant Piezomagnetism and Noncollinear Spin Current*, *Nat. Commun.* **12**, 2846 (2021).
- [13] K. Samanta, M. Ležaić, M. Merte, F. Freimuth, S. Blügel, and Y. Mokrousov, *Crystal Hall and Crystal Magneto-Optical Effect in Thin Films of SrRuO₃*, *J. Appl. Phys.* **127**, 213904 (2020).
- [14] M. Naka, S. Hayami, H. Kusunose, Y. Yanagi, Y. Motome, and H. M. Seo, *Anomalous Hall Effect in κ Organic Antiferromagnets*, *Phys. Rev. B* **102**, 075112 (2020).
- [15] X. Zhou, W. Feng, X. Yang, G.-Y. Guo, and Y. Yao, *Crystal Chirality Magneto-Optical Effects in Collinear Antiferromagnets*, *Phys. Rev. B* **104**, 024401 (2021).
- [16] R. González-Hernández, L. Šmejkal, K. Vyborny, Y. Yahagi, J. Sinova, T. Jungwirth, and J. Zelezny, *Efficient Electrical Spin Splitter Based on Nonrelativistic Collinear Antiferromagnetism*, *Phys. Rev. Lett.* **126**, 127701 (2021).
- [17] L. Šmejkal, A. B. Hellenes, R. González-Hernández, J. Sinova, and T. Jungwirth, *Giant and Tunneling Magneto-resistance in Unconventional Collinear Antiferromagnets with Nonrelativistic Spin-Momentum Coupling*, *Phys. Rev. X* **12**, 011028 (2022).
- [18] D.-F. Shao, S.-H. Zhang, M. Li, C.-B. Eom, and E. Y. Tsymbal, *Spin-Neutral Currents for Spintronics*, *Nat. Commun.* **12**, 7061 (2021).
- [19] Z. Feng *et al.*, *Observation of the Crystal Hall Effect in a Collinear Antiferromagnet*, arXiv:2002.08712.
- [20] A. Bose *et al.*, *Tilted Spin Current Generated by the Collinear Antiferromagnet Ruthenium Dioxide*, *Nat. Electron.* **5**, 267 (2022).
- [21] H. Bai *et al.*, *Observation of Spin Splitting Torque in a Collinear Antiferromagnet RuO₂*, *Phys. Rev. Lett.* **128**, 197202 (2022).
- [22] S. Karube *et al.*, *Observation of Spin-Splitter Torque in Collinear Antiferromagnetic RuO₂*, arXiv:2111.07487.
- [23] W. F. Brinkman and R. J. Elliott, *Theory of Spin-Space Groups*, *Proc. R. Soc. A* **294**, 343 (1966).
- [24] D. Litvin and W. Opechowski, *Spin Groups*, *Physica (Amsterdam)* **76**, 538 (1974).
- [25] D. B. Litvin, *Spin Point Groups*, *Acta Crystallogr., Sect. A* **33**, 279 (1977).
- [26] L. Néel, *Magnetism and Local Molecular Field*, *Science* **174**, 985 (1971).
- [27] P. W. Anderson, *The Resonating Valence Bond State in La₂CuO₄ and Superconductivity*, *Science* **235**, 1196 (1987).
- [28] M.-T. Suzuki, T. Koretsune, M. Ochi, and R. Arita, *Cluster Multipole Theory for Anomalous Hall Effect in Antiferromagnets*, *Phys. Rev. B* **95**, 094406 (2017).
- [29] C. J. Bradley and A. P. Cracknell, *The Mathematical Theory of Symmetry in Solids* (Oxford University Press, New York, 1972).
- [30] See Supplemental Material at <http://link.aps.org/supplemental/10.1103/PhysRevX.12.031042> for comparison of relativistic magnetic symmetries and nonrelativistic spin symmetries, details of the derivation of spin group categorization and symmetry delimitation of collinear magnets, altermagnetic model Hamiltonians, summary of symmetry properties of altermagnets, and calculated band-structures of selected candidate altermagnets.
- [31] L. Landau and E. Lifshitz, *Electrodynamics of Continuous Media*, 2nd ed., Course of Theoretical Physics Vol. 8 (Pergamon Press, Oxford, 1965).
- [32] E. Turov, *Physical Properties of Magnetically Ordered Crystals* (Academic Press, New York, 1965).
- [33] N. V. Shubnikov and A. V. Belov, *Colored Symmetry* (Macmillan Publishers, New York, 1964).
- [34] B. A. Tavger and V. M. Zaitsev, *Magnetic Symmetry of Crystals*, *Sov. Phys. JETP* **3**, 430 (1956).
- [35] D. B. Litvin, *Magnetic Group Tables* (International Union of Crystallography, Chester, England, 2013).
- [36] L. Šmejkal, Y. Mokrousov, B. Yan, and A. H. MacDonald, *Topological Antiferromagnetic Spintronics*, *Nat. Phys.* **14**, 242 (2018).
- [37] H. Watanabe, H. C. Po, and A. Vishwanath, *Structure and Topology of Band Structures in the 1651 Magnetic Space Groups*, *Sci. Adv.* **4**, eaat8685 (2018).
- [38] Y. Xu, L. Elcoro, Z.-D. Song, B. J. Wieder, M. G. Vergniory, N. Regnault, Y. Chen, C. Felser, and B. Andrei Bernevig, *High-Throughput Calculations of Magnetic Topological Materials*, *Nature (London)* **586**, 702 (2020).
- [39] S. V. Gallego, J. Manuel Perez-Mato, L. Elcoro, E. S. Tasci, R. M. Hanson, K. Momma, M. I. Aroyo, and G. Madariaga, *MAGNDATA: Towards a Database of Magnetic Structures. I. The Commensurate Case*, *J. Appl. Crystallogr.* **49**, 1750 (2016).

- [40] A. F. Andreev and V. Marchenko, *Symmetry and the Macroscopic Dynamics of Magnetic Materials*, *Usp. Fiz. Nauk* **130**, 39 (1980).
- [41] A. Corticelli, R. Moessner, and P. A. McClarty, *Spin-Space Groups and Magnon Band Topology*, *Phys. Rev. B* **105**, 064430 (2022).
- [42] P.-J. Guo, Y.-W. Wei, K. Liu, Z.-X. Liu, and Z.-Y. Lu, *Eightfold Degenerate Fermions in Two Dimensions*, *Phys. Rev. Lett.* **127**, 176401 (2021).
- [43] P. Liu, J. Li, J. Han, X. Wan, and Q. Liu, *Spin-Group Symmetry in Magnetic Materials with Negligible Spin-Orbit Coupling*, *Phys. Rev. X* **12**, 021016 (2022).
- [44] J. Yang, Z.-X. Liu, and C. Fang, *Symmetry Invariants of Spin Space Groups in Magnetic Materials*, [arXiv:2105.12738](https://arxiv.org/abs/2105.12738).
- [45] P. Liu, J. Han, and Q. Liu, *Flavor Weyl Fermions Protected by $SU(2)$ Isospin Symmetry in Spin-Orbit-Free Antiferromagnetic Semimetals*, [arXiv:2107.09984](https://arxiv.org/abs/2107.09984).
- [46] P. M. Lenggenhager, X. Liu, T. Neupert, and T. Bzdušek, *Triple Nodal Points Characterized by Their Nodal-Line Structure in All Magnetic Space Groups*, *Phys. Rev. B* **106**, 085128 (2022).
- [47] W. H. Kleiner, *Space-Time Symmetry of Transport Coefficients*, *Phys. Rev.* **142**, 318 (1966).
- [48] R. Ramazashvili, *Kramers Degeneracy in a Magnetic Field and Zeeman Spin-Orbit Coupling in Antiferromagnetic Conductors*, *Phys. Rev. B* **79**, 184432 (2009).
- [49] P. Tang, Q. Zhou, G. Xu, and S.-C. Zhang, *Dirac Fermions in an Antiferromagnetic Semimetal*, *Nat. Phys.* **12**, 1100 (2016).
- [50] L. Šmejkal, J. Železný, J. Sinova, and T. Jungwirth, *Electric Control of Dirac Quasiparticles by Spin-Orbit Torque in an Antiferromagnet*, *Phys. Rev. Lett.* **118**, 106402 (2017).
- [51] L. Šmejkal, T. Jungwirth, and J. Sinova, *Route towards Dirac and Weyl Antiferromagnetic Spintronics*, *Phys. Status Solidi RRL* **11**, 1700044 (2017).
- [52] K. Yamauchi, P. Barone, and S. Picozzi, *Bulk Rashba Effect in Multiferroics: A Theoretical Prediction for BiCoO_3* , *Phys. Rev. B* **100**, 245115 (2019).
- [53] H. A. Kramers, *Théorie générale de la rotation paramagnétique dans les cristaux*, *Proc. Amsterdam Acad.* **33**, 959 (1930).
- [54] E. Wigner, *Ueber die Operation der Zeitumkehr in der Quantenmechanik*, *Nach. Ges. Wiss. Göttingen Math.-Phys. Kl.* **1932**, 546 (1932).
- [55] A. S. Núñez, R. A. Duine, P. Haney, and A. H. MacDonald, *Theory of Spin Torques and Giant Magnetoresistance in Antiferromagnetic Metals*, *Phys. Rev. B* **73**, 214426 (2006).
- [56] C. Sürgers, G. Fischer, G. Winkel, and H. V. Löhneysen, *Large Topological Hall Effect in the Non-Collinear Phase of an Antiferromagnet*, *Nat. Commun.* **5**, 3400 (2014).
- [57] C. Sürgers, W. Kittler, T. Wolf, and H. V. Löhneysen, *Anomalous Hall Effect in the Noncollinear Antiferromagnet Mn_5Si_3* , *AIP Adv.* **6**, 055604 (2016).
- [58] N. J. Ghimire, A. S. Botana, J. S. Jiang, J. Zhang, Y.-S. Chen, and J. F. Mitchell, *Large Anomalous Hall Effect in the Chiral-Lattice Antiferromagnet CoNb_3S_6* , *Nat. Commun.* **9**, 3280 (2018).
- [59] S. I. Pekar and E. I. Rashba, *Combined Resonance in Crystals in Inhomogeneous Magnetic Fields*, *J. Exp. Theor. Phys.* **20**, 1927 (1965).
- [60] S. A. Egorov and R. A. Evarestov, *Colossal Spin Splitting in the Monolayer of the Collinear Antiferromagnet MnF_2* , *J. Phys. Chem. Lett.* **12**, 2363 (2021).
- [61] J. A. Sobota, Y. He, and Z.-X. Shen, *Angle-Resolved Photoemission Studies of Quantum Materials*, *Rev. Mod. Phys.* **93**, 025006 (2021).
- [62] X. Marti *et al.*, *Room-Temperature Antiferromagnetic Memory Resistor*, *Nat. Mater.* **13**, 367 (2014).
- [63] J. Li, Y. Li, S. Du, Z. Wang, B.-L. Gu, S.-C. Zhang, K. He, W. Duan, and Y. Xu, *Intrinsic Magnetic Topological Insulators in van der Waals Layered MnBi_2Te_4 -Family Materials*, *Sci. Adv.* **5**, eaaw5685 (2019).
- [64] H. J. Elmers *et al.*, *Néel Vector Induced Manipulation of Valence States in the Collinear Antiferromagnet Mn_2Au* , *ACS Nano* **14**, 17554 (2020).
- [65] R. Winkler, *Spin-Orbit Coupling Effects in Two-Dimensional Electron and Hole Systems*, Springer Tracts in Modern Physics Vol. 191 (Springer, Berlin, 2003).
- [66] Y. Noda, K. Ohno, and S. Nakamura, *Momentum-Dependent Band Spin Splitting in Semiconducting MnO_2 : A Density Functional Calculation*, *Phys. Chem. Chem. Phys.* **18**, 13294 (2016).
- [67] S. López-Moreno, A. H. Romero, J. Mejía-López, A. Muñoz, and I. V. Roshchin, *First-Principles Study of Electronic, Vibrational, Elastic, and Magnetic Properties of FeF_2 as a Function of Pressure*, *Phys. Rev. B* **85**, 134110 (2012).
- [68] T. Okugawa, K. Ohno, Y. Noda, and S. Nakamura, *Weakly Spin-Dependent Band Structures of Antiferromagnetic Perovskite LaMO_3 ($M = r, \text{Mn}, \text{Fe}$)*, *J. Phys. Condens. Matter* **30**, 075502 (2018).
- [69] W. Kobayashi, *Transport Properties of Quasi-One-Dimensional KRu_4O_8* , *Phys. Rev. B* **79**, 155116 (2009).
- [70] T. Toriyama, M. Watanabe, T. Konishi, and Y. Ohta, *Quasi-One-Dimensional Electronic Structure of Hollandite Ruthenate $\text{K}_2\text{Ru}_8\text{O}_{16}$* , *Phys. Rev. B* **83**, 195101 (2011).
- [71] K. Dewhurst, ELK code, <http://elk.sourceforge.net>.
- [72] D. I. Khomskii, *Transition Metal Compounds* (Cambridge University Press, Cambridge, England, 2014).
- [73] K. Ishizaka *et al.*, *Giant Rashba-Type Spin Splitting in Bulk BiTeI* , *Nat. Mater.* **10**, 521 (2011).
- [74] I. J. Park, S. Kwon, and R. K. Lake, *Effects of Filling, Strain, and Electric Field on the Néel Vector in Antiferromagnetic CrSb* , *Phys. Rev. B* **102**, 224426 (2020).
- [75] J. Yuan, Y. Song, X. Xing, and J. Chen, *Magnetic Structure and Uniaxial Negative Thermal Expansion in Antiferromagnetic CrSb* , *Dalton Trans.* **49**, 17605 (2020).
- [76] C. Lane, J. W. Furness, I. G. Buda, Y. Zhang, R. S. Markiewicz, B. Barbiellini, J. Sun, and A. Bansil, *Antiferromagnetic Ground State of La_2CuO_4 : A Parameter-Free Ab Initio Description*, *Phys. Rev. B* **98**, 125140 (2018).
- [77] G. Tenasini *et al.*, *Giant Anomalous Hall Effect in Quasi-Two-Dimensional Layered Antiferromagnet $\text{Co}_1/3\text{NbS}_2$* , *Phys. Rev. Research* **2**, 023051 (2020).
- [78] L. Vistoli *et al.*, *Giant Topological Hall Effect in Correlated Oxide Thin Films*, *Nat. Phys.* **15**, 67 (2019).
- [79] J. Wu, A. T. Bollinger, X. He, and I. Božović, *Spontaneous Breaking of Rotational Symmetry in Copper Oxide Superconductors*, *Nature (London)* **547**, 432 (2017).

- [80] C. Chappert, A. Fert, and F. N. Van Dau, *The Emergence of Spin Electronics in Data Storage*, *Nat. Mater.* **6**, 813 (2007).
- [81] D. C. Ralph and M. D. Stiles, *Spin Transfer Torques*, *J. Magn. Magn. Mater.* **320**, 1190 (2008).
- [82] S. Bhatti, R. Sbiaa, A. Hirohata, H. Ohno, S. Fukami, and S. N. Piramanayagam, *Spintronics Based Random Access Memory: A Review*, *Mater. Today* **20**, 530 (2017).
- [83] A. Manchon, J. Zelezny, I. M. Miron, T. Jungwirth, J. Sinova, A. Thiaville, K. Garello, and P. Gambardella, *Current-Induced Spin-Orbit Torques in Ferromagnetic and Antiferromagnetic Systems*, *Rev. Mod. Phys.* **91**, 035004 (2019).
- [84] J. R. Schaibley, H. Yu, G. Clark, P. Rivera, J. S. Ross, K. L. Seyler, W. Yao, and X. Xu, *Valleytronics in 2D Materials*, *Nat. Rev. Mater.* **1**, 16055 (2016).
- [85] S. Hayami, M. Yatsushiro, Y. Yanagi, and H. Kusunose, *Classification of Atomic-Scale Multipoles under Crystallographic Point Groups and Application to Linear Response Tensors*, *Phys. Rev. B* **98**, 165110 (2018).
- [86] C. Wu, K. Sun, E. Fradkin, and S.-C. Zhang, *Fermi Liquid Instabilities in the Spin Channel*, *Phys. Rev. B* **75**, 115103 (2007).
- [87] Q. Si, R. Yu, and E. Abrahams, *High-Temperature Superconductivity in Iron Pnictides and Chalcogenides*, *Nat. Rev. Mater.* **1**, 16017 (2016).
- [88] K. Flensberg, F. von Oppen, and A. Stern, *Engineered Platforms for Topological Superconductivity and Majorana Zero Modes*, *Nat. Rev. Mater.* **6**, 944 (2021).
- [89] L. Smejkal, J. Sinova, and T. Jungwirth, *Emerging Research Landscape of Altermagnetism*, arXiv:2204.10844.
- [90] J. E. Moore, *The Birth of Topological Insulators*, *Nature (London)* **464**, 194 (2010).
- [91] A. Schofield, *There and Back Again: From Magnets to Superconductors*, *Physics* **2**, 93 (2009).
- [92] L. Classen, A. V. Chubukov, C. Honerkamp, and M. M. Scherer, *Competing Orders at Higher-Order van Hove Points*, *Phys. Rev. B* **102**, 125141 (2020).
- [93] R. A. Borzi, S. A. Grigera, J. Farrell, R. S. Perry, S. J. S. Lister, S. L. Lee, D. A. Tennant, Y. Maeno, and A. P. Mackenzie, *Formation of a Nematic Fluid at High Fields in Sr₃Ru₂O₇*, *Science* **315**, 214 (2007).